energies

MDPI

Article

Energy Consumption and Saved Emissions of a Hydrogen Power System for Ultralight Aviation: A Case Study

Teresa Donateo [1,*], Andrea Graziano Bonatesta [1], Antonio Ficarella [1] and Leonardo Lecce [2]

[1] Department of Engineering for Innovation, University of Salento, Via per Monteroni, 73100 Lecce, Italy; antonio.ficarella@unisalento.it (A.F.)
[2] Novotech Aerospace Advanced Technology S.R.L., Strada Provinciale 143 KM. 2, 74020 Avetrana, Italy; leonardo.lecce@novotech.it
* Correspondence: teresa.donateo@unisalento.it; Tel.: +39-0832297754

Abstract: The growing concern about climate change and the contemporary increase in mobility requirements call for faster, cheaper, safer, and cleaner means of transportation. The retrofitting of fossil-fueled piston engine ultralight aerial vehicles to hydrogen power systems is an option recently proposed in this direction. The goal of this investigation is a comparative analysis of the environmental impact of conventional and hydrogen-based propulsive systems. As a case study, a hybrid electric configuration consisting of a fuel cell with a nominal power of about 30 kW, a 6 kWh LFP battery, and a pressurized hydrogen vessel is proposed to replace a piston prop configuration for an ultralight aerial vehicle. Both power systems are modeled with a backward approach that allows the efficiency of the main components to be evaluated based on the load and altitude at every moment of the flight with a time step of 1 s. A typical 90 min flight mission is considered for the comparative analysis, which is performed in terms of direct and indirect emissions of carbon dioxide, water, and pollutant substances. For the hydrogen-based configuration, two possible strategies are adopted for the use of the battery: charge sustaining and charge depleting. Moreover, the effect of the altitude on the parasitic power of the fuel cell compressor and, consequently, on the net efficiency of the fuel cell system is taken into account. The results showed that even if the use of hydrogen confines the direct environmental impact to the emission of water (in a similar quantity to the fossil fuel case), the indirect emissions associated with the production, transportation, and delivery of hydrogen and electricity compromise the desired achievement of pollutant-free propulsion in terms of equivalent emissions of CO_2 and VOCs if hydrogen is obtained from natural gas reforming. However, in the case of green hydrogen from electrolysis with wind energy, the total (direct and indirect) emissions of CO_2 can be reduced up to 1/5 of the fossil fuel case. The proposed configuration has the additional advantage of eliminating the problem of lead, which is used as an additive in the AVGAS 100LL.

Keywords: hydrogen propulsion; fuel cell; balance of plant; indirect emissions; ultralight aviation

Citation: Donateo, T.; Bonatesta, A.G.; Ficarella, A.; Lecce, L. Energy Consumption and Saved Emissions of a Hydrogen Power System for Ultralight Aviation: A Case Study. *Energies* **2024**, *17*, 3272. https://doi.org/10.3390/en17133272

Academic Editors: Vladislav A. Sadykov and Jianbing Gao

Received: 23 May 2024
Revised: 20 June 2024
Accepted: 1 July 2024
Published: 3 July 2024

1. Introduction

The air transport industry plans to become carbon neutral by 2050 by eliminating fossil-fuel-burning engines in all transportation categories [1,2]. Fossil fuels derived from petroleum are commonly used in aerospace propulsion; in particular, kerosene and Avgas (aviation gasoline) are burned in turbine and piston engines, respectively. Small piston aircraft represent a small part of the overall airspace, and for this reason, they are often neglected in regulatory emissions control. However, since the environmental impact of large commercial engines has decreased in recent years, it has become important to assess the contribution of piston aircraft too [3,4].

Avgas 100LL, commonly adopted in ultralight aviation, produces 3.05 kg of CO_2 [5] per unit weight of fuel used and several pollutant emissions, including NO_x, HC, and CO, as outcomes of the internal combustion processes. Moreover, it contains a lead-based

anti-knock compound to achieve the desired octane rating for piston engines, which causes damage to human health and the environment [6,7].

To reduce the environmental impact of aviation, fully electric aircraft powered by batteries have been proposed, but their actual application is limited to Unmanned Aerial Vehicles (UAVs) and short-haul vehicles for Urban Air Mobility. In fact, this solution cannot be adopted for general aviation because of the limited specific energy of today's batteries, which, in turn, limits the flying time.

Hydrogen has the potential to solve the problem of reducing the environmental impact while guaranteeing longer endurance than battery-based electric propulsion systems [8]. It can be used as a replacement for kerosene in turbine engines or feed fuel cells in place of piston engines in small airplanes. Fuel cells are electrochemical devices that convert the chemical energy of a fuel, often hydrogen, into electric energy with different possible technologies, among which PEMFCs (Proton Exchange Membrane Fuel Cells) are the most commonly adopted in transportation systems thanks to their relatively higher specific power. PEMFCs have the advantage of higher efficiency than thermal engines and produce only water and heat as by-products, while burning hydrogen in internal combustion engines inevitably generates harmful emissions of nitrogen oxides. Moreover, they are silent and low-vibration devices [9,10].

PEMFC power systems have been proposed for all sizes of aerial vehicles, from small UAVs to commercial flights. This investigation focuses on ultralight aviation, where only a few research projects have been carried out in the recent past for the development of hydrogen-based propulsion systems (see Table 1). In these projects, fuel cells are always combined with batteries in hybrid electric configurations. In fact, fuel cells are penalized in terms of power density when compared with batteries and, in particular, with NMC and LFP lithium batteries, while the energy density of compressed hydrogen is much higher than the Wh/kg that can be achieved by lithium batteries.

Another critical aspect of the application of fuel cells to the aerospace field is the control of temperature. The fuel cell stacks adopted in these projects are usually liquid-cooled. This allows more efficient control of temperature, but at the expense of a higher mass, volume, and complexity of the Balance Of Plant (BOP) than in air-cooled configurations [11]. In the Antares and HY4 projects, the adoption of air-cooled High-Temperature Proton Exchange Fuel Cells (HTPEMFCs) is proposed to simplify the BOP.

Table 1. List of projects adopting PEMFCs for manned aerial vehicles.

Project	Aircraft	MaxTakeOff Weight	FC Power	Stack Cooling	Hydrogen Storage	Source
Boeing Phantom	Motor glider	770 kg	20 kW	Liquid-cooled	Pressurized at 350 bar	[12]
ENFICA-FC	Ultralight	554 kg	20 kW	Liquid-cooled	Pressurized (no details)	[13]
Sigma-4	Ultralight	650 kg	35 kW	Liquid-cooled	Pressurized (no details)	[14]
Antares DLR-H2	Motor glider	825 kg	3 × 10 kW	Air-cooled vs. liquid-cooled	Pressurized at 350 bar	[15]
H2fly Pipistrel HY4 2016	4 pax	1500 kg	4 × 10 kW	Air-cooled	Liquefied	[16]

Regarding hydrogen storage, pressurized vessels are generally adopted. Unfortunately, it was not possible to find many details about the specifications of the proposed power systems of these prototypes and, in particular, the storing pressure. However, it can be assumed to vary between 20 MPa and 70 MPa [17]. Liquefied hydrogen solutions are adopted in larger aircraft (see, for example, H2Fly by Pipistrel) [16].

Unlike hydrogen cars, fuel cell-powered aircraft are still at an early research and development stage [18] also because of the lack of a hydrogen infrastructure; therefore, it is not yet possible to assess the economic viability of such power systems for aerospace applications. In a previous investigation by the authors [19], the estimated cost for the replacement of a Rotax 912ULS (which costs about kEUR 26 according to [20]) with a hybrid electric power system with a fuel cell is about kEUR 100.

This investigation is performed in the framework of the SERENA project, whose goal is the development of a full-electric modular powertrain for general aviation, integrating batteries and hydrogen fuel cell technology. Modularity offers scalable solutions within a reasonable range of propulsive power, accommodating varying operational needs and potential future adaptations. The partnership of the SERENA project includes the Aerospace Technologic District (DTA-Scarl), EnginSoft Spa, Novotec S.R.L., and the University of Salento. The main activities of the project comprise the following:

1. The development of a modular hybrid electric powertrain with fuel cells;
2. Estimate of environmental benefits in terms of greenhouse and pollutant gas emissions;
3. The design, assembly, verification, and validation of a scaled demonstrator (one module of the whole power system);
4. Bench testing the propulsion system demonstrator;
5. The development of a digital twin of the full-scale power system validated on the physical mock-up;
6. Virtual integration of the hydrogen power system on aircraft;
7. The definition of requirements and analysis of challenges in terms of safety and certification of the propulsion system, with particular reference to the use of hydrogen as the main energy carrier.

This investigation addresses item 2 based on the preliminary design of a modular hybrid electric powertrain developed in a previous investigation [19].

The environmental benefit of utilizing fuel cells over conventional fossil fuels and battery-based power systems is not a novelty in the scientific literature, especially for road transportation [21].

Çalışır [22] performed a LCA analysis of a hydrogen hybrid electric system with fuel cells versus a lithium polymer battery drive system for a fixed-wing unmanned aerial vehicle. Çalışır found that emissions of carbon dioxides are reduced by 6.95% with the adoption of the fuel cell configuration. In particular, a configuration with a PEM fuel cell was found to guarantee a lower takeoff weight and life cycle cost than a pure battery power system for flight endurance between 40 min and 2.1 h [23]. However, the LCA analysis in these studies was performed for GHGs only.

However, the scientific literature on the use of hydrogen in ultralight aviation, a detailed analysis of saved greenhouse gases (GHGs), and pollutant emissions in ultralight aviation are missing to the best of the authors' knowledge. To fill this gap, the authors applied the emission factors retrieved in the scientific literature for both gasoline and hydrogen fuels to a specific test case related to ultralight recreational aircraft. In particular, the retrofitting of the Novotech Seagull from a conventional powertrain consisting of a Rotax 912UL engine fueled with Avgas 100LL to a hybrid fuel cell–battery power system is addressed in this paper. The scientific contribution is given by the detailed analysis of the energy flows in the different phases of the mission and the estimation of direct and indirect emissions saved with the retrofitting per single mission.

This paper is structured as follows: Section 2 describes the Seagull aircraft and the modeling approach used for the original and hydrogen-based power systems. Section 3 explains how direct and indirect emissions are computed for the two power systems. The results of the computations in terms of energy flows and pollutant emissions are presented and discussed in Section 4.

2. Reference Aircraft and Energy Flow Analysis

The Seagull is a two-seat high-wing amphibian vehicle equipped with a piston prop configuration (Figure 1). The main specifications of the aircraft and its propulsive system are shown in Table 2 for the original configuration.

Figure 1. The Novotech Seagull.

Table 2. Technical specifications of the Seagull.

Parameter	Value
Wingspan	10.5 m
Wing area	13.5 m^2
Max gross weight	700 kg
Maximum zero fuel weight	650 kg
Maximum baggage weight	20 kg
Pay weight	80 kg
Power loading	6.5 kg/HP
Engine	Rotax 912UL
Fuel tank capacity	70 L (50 kg)

The polar of the Seagull, i.e., the correlation between the drag coefficient c_D and the lift coefficient c_L, is shown in Figure 2.

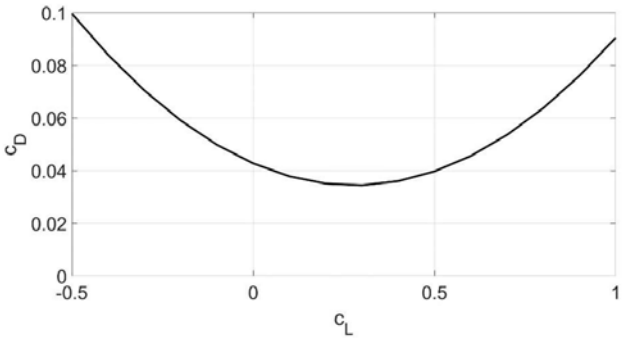

Figure 2. The polar of the Seagull.

The mission considered in this investigation consists of six phases, as shown in Figure 3, with a maximum flight altitude of 1830 m (6000 ft). The specifications of the mission are reported in Table 3; more details about the choice of this mission can be found in [24].

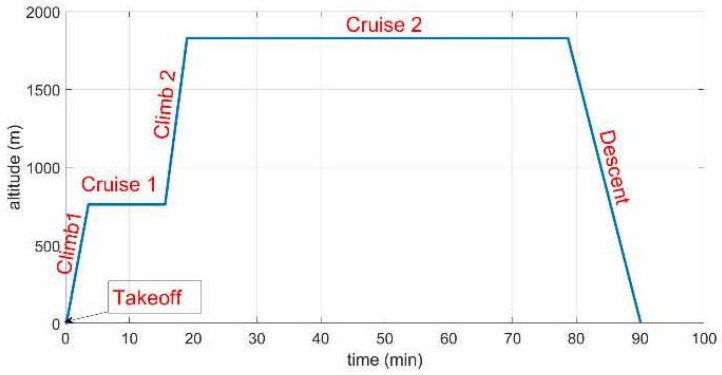

Figure 3. The flight envelop of the proposed mission.

Table 3. Specifications of the mission.

Parameter	Value
Pitch setting	18.5°
Lift-off speed	25 m/s
Rate of climb 1	4.2 m/s
Rate of climb 2	5.87 m/s
Rate of descent	3.03 m/s
True air speed	41.7 m/s
Altitude of cruise 1/cruise 2	2500 ft/6000 ft
Total flight time	90 min

An adjustable pitch propeller (a three-blade DUC Helices Flash with a diameter of 1.52 m) was adopted in both configurations.

The efficiency map of the propeller is displayed in Figure 4, where $J = V_\infty / n_{prop} D_{prop}$ is the advance ratio calculated from the values of true airspeed V_∞, air density ρ, propeller speed in rps, n_{prop}, and propeller diameter D_{prop}.

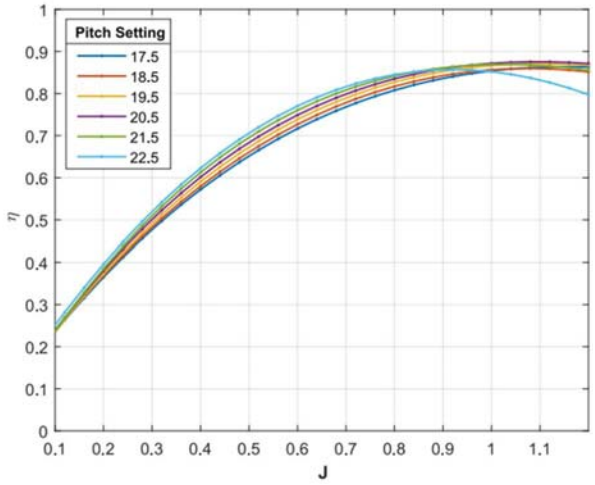

Figure 4. The efficiency map of the propeller.

2.1. Propulsive Power

The takeoff phase is simulated with a forward approach, with the engine (original configuration) or motors (new power system) working at their maximum power. The average thrust is used to calculate the acceleration during the takeoff phase. The resulting takeoff time is 60 s for the original configuration and less than 10 s for the hybrid electric configuration.

The simulations were performed with an in-house simulation code named PLA.N.E.S. [25], developed by some of the authors and implemented in Matlab R2023b. This software tool is based on a backward simulation approach, where the mission envelope is discretized with a time step of 1 s. The flight envelope in Figure 3 and the specifications in Table 3 are used to calculate the forces acting on the plane in each phase of the mission by applying the standard equations of aerodynamics [26]. In particular, the thrust force is used to calculate the propulsive power P_{prop} and the advance ratio J for the propeller model. By using the propeller efficiency map (Figure 4), the brake power is calculated. This is the input to the power system models described later for the conventional and hydrogen hybrid electric power systems.

Using the efficiency map of the propeller, it is possible to obtain the values of propeller efficiency and speed in the six phases of the mission and, therefore, the request of mechanical power P_{mech} at the propeller axis:

$$P_{mech} = \frac{P_{prop}}{\eta_{prop}\left(n_{prop}, \alpha_{pitch}\right)} \quad (1)$$

where α_{pitch} is the selected pitch angle (18.5° in this investigation).

The method is summarized in Figure 5 and explained in detail in [27].

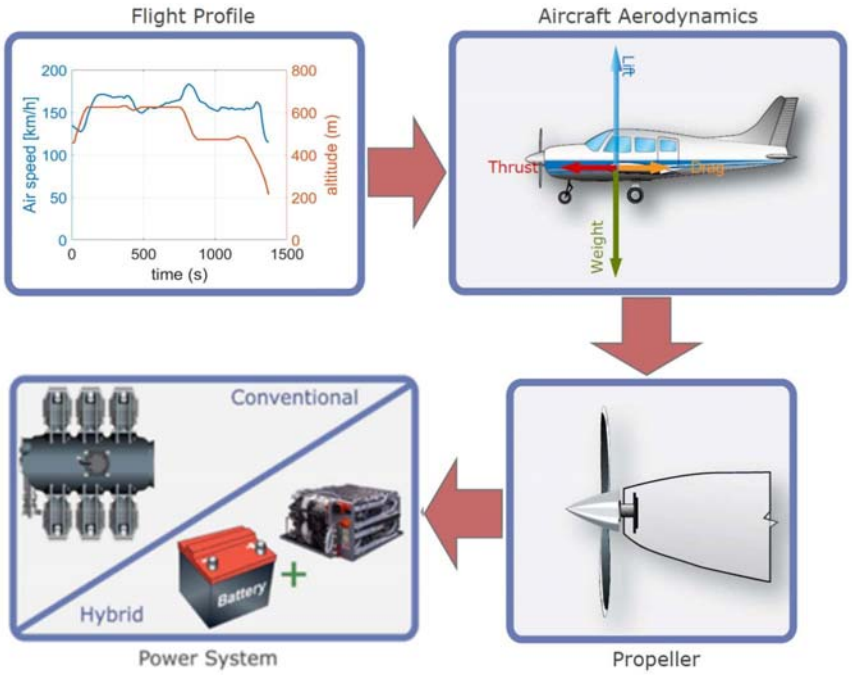

Figure 5. Backward simulation approach.

The values of propulsive power and propeller advance ratio, calculated with the proposed method in the six phases of the mission, are shown in Table 4.

Table 4. Propulsive power and propeller advance ratio (original/new power system).

	Time Original/New	Propulsive Power Original/New	Propeller Advance Ratio	Propeller Efficiency
	s	kW	-	%
Takeoff	60/10	46/82	0.35	58
Climb 1	206	45.5	0.72	85
Cruise 1	670	21.5	0.82	71
Climb 2	206	54.7	0.66	89
Cruise 2	3579	21.5	0.82	71
Descent	684	4.3	1.1	54

2.2. Energy Flows in the Original Configuration

In the original power system, the mechanical power P_{mech} is generated by a Rotax 912UL piston engine, which is connected to the propeller through a transmission ratio equal to 2.43 (see Figure 6).

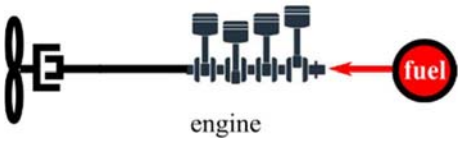

Figure 6. Original power system.

The engine has a nominal power of 73.5 kW at 5800 rpm. The Wide-Open Throttle (WOT) torque curve and the fuel efficiency map of the engine, shown in Figure 7, were obtained by using the data of the manufacturer at full throttle and along the propeller line [27,28]. More details on how the map was obtained can be found in [29]. Since the performance of the engine is affected by the altitude, the figure shows the WOT at sea level and the maximum altitude achieved in the proposed mission at cruise 2 (6000 ft). The working points of the engine in the six phases of the mission are reported as red circles. As shown in [17], up to 6000 ft, the engine efficiency is weakly affected by the altitude, so this effect is neglected in the present investigation.

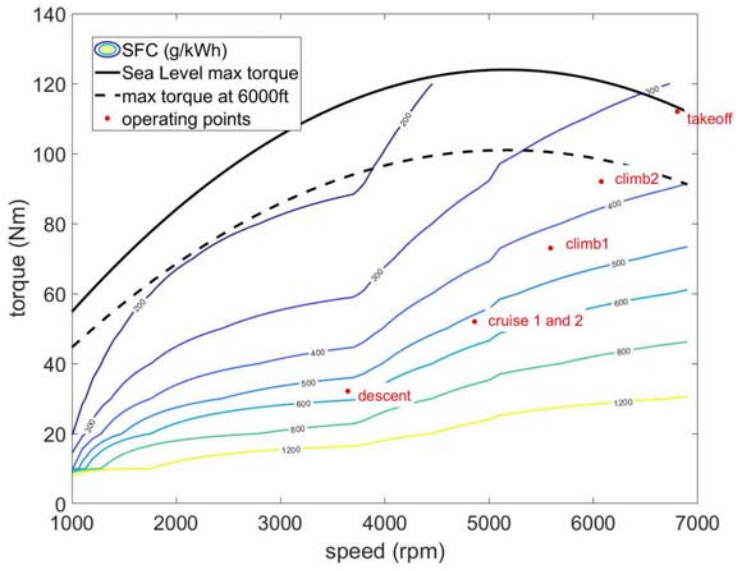

Figure 7. Wide-open throttle torque and efficiency map of the Rotax 912ULS [29] with working points during the mission.

Using the efficiency map in Figure 7, the fuel flow rate FFR is computed as follows:

$$FFR = \frac{P_{ice}}{\eta_{ice}(n_{ice})LHV} \quad (2)$$

where $\eta_{ice}(n_{ice})$ is the engine efficiency obtained from Figure 7 for each working point. LHV is the lower heating value of Avgas100LL (43.5 MJ/kg), and P_{ice} is the engine brake power.

2.3. Energy Flows in the New Power System

In the hydrogen hybrid electric power system, the same propeller is assumed to be connected to two twin electric motors with a gear ratio of 2. The EMRAX228 electric motor (EMRAX, Kamnkik, Slovenia) presents the efficiency map in Figure 8 that was obtained from the manufacturer.

The electric power request of the motor is supplied by the fuel cell and the battery (Figure 9).

The adoption of hybrid electric configurations also allows for safer operation thanks to the possibility of completing the mission with the battery in case of fuel cell failure (or engine failure). This is particularly critical in ultralight aviation, where single-engine prop systems are adopted, and this causes a high number of (generally deathly) accidents caused by engine failure [29]. On the other hand, the use of hydrogen introduces critical safety issues that are to be solved by an accurate design and control of the hydrogen vessel [30] and of the whole hydrogen path. This analysis is included in the activities of the SERENA project and will be considered in future investigations of the partnership.

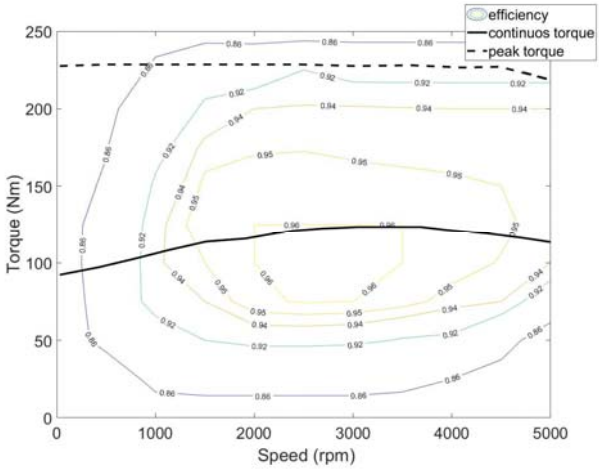

Figure 8. Performance curves and efficiency map of the electric machine (digitalized from the manual).

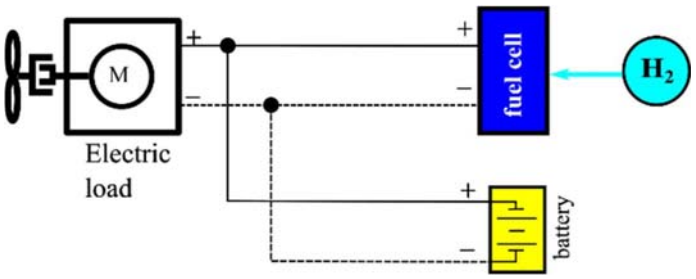

Figure 9. Hydrogen power system.

A careful analysis of the Seagull architecture was performed in [24] to obtain feasible values of the total mass and volume of the proposed power system, which were found to be 200 kg and 200 L, respectively, for the whole system.

The use of the battery in the mission is regulated by a very simple rule-based Energy Management Strategy (EMS). The battery is used when the mission requirement exceeds a threshold level for the fuel cell. Note that the battery can be charged in the last phases of the mission to achieve a Charge Sustaining (CS) behavior and avoid the need to charge the battery between two consecutive flights. However, a charge-depleting approach can also be adopted.

The three main components of the new power system, namely the fuel cell system, the battery, and the hydrogen vessel, were sized in a previous investigation [19,24] with a procedure aimed at minimizing the mass and volume of the new power system. For the hydrogen vessel, the storing pressure determines a tradeoff between the occupied volume (which decreases with pressure) and the cylinder thickness and weight (because of the need to withstand a higher gas pressure). Since the occupied space of the power system was found to be the most difficult goal to achieve [19,24], a high hydrogen pressure (700 bar) was preferred for this investigation. However, the 350-bar solution is also under consideration in the project.

In that investigation, two optimal configurations were identified with (CS) and without (CD) battery charge during the flight. Their specifications are summarized in Table 5.

In this investigation, a configuration with two twin modules able to perform both CS and CD operations has been adopted. The modular structure for a fuel cell system (MFCS) has the advantage of meeting the demands of diversification applications, especially high power demands (>200 kW), providing more redundancy than a single fuel cell system (SFCS) [31–33]. This redundancy can be applied to enable the degraded mode operation, reduce the hydrogen consumption, act on the aging, and increase the reliability. Moreover, modularity allows a longer lifetime than a SFCS and higher efficiency because the MFCS can provide several optimal powers through different distribution possibilities [34]. On the

other hand, the cost of the PEM MFCS is one of the core barriers to commercialization applications and, there are some challenges to practical applications in terms of the complexity of the BOP [34].

Table 5. The results of the design procedure performed in [24].

	CD (w/o Onboard Battery Charge)	CS (Full On-Board Charging)
FC size (kW)	32.5	35.7
Battery size (kWh)	5.9	5
Tank volume (L) at 700 bar	57.4	65.4

2.3.1. The Fuel Cell Model

For each module, the consumption of hydrogen is calculated with a simple model based on the performance data of the stack and compressor qualitatively reported in Figure 10 because of a confidentiality agreement with the fuel cell manufacturer.

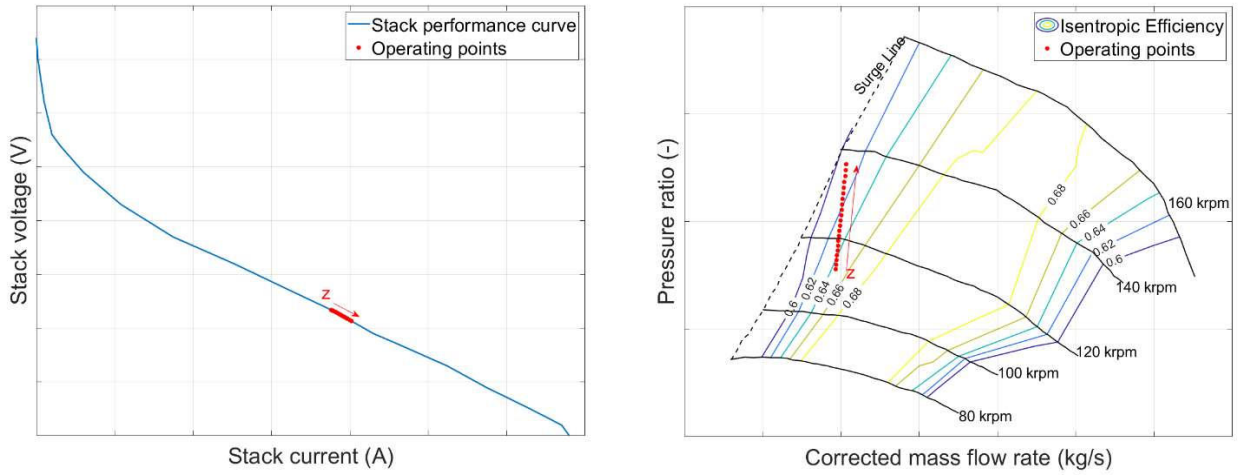

(**a**) (**b**)

Figure 10. Operating points of fuel cells and compressor (red circles) at a constant net power (15 kW) when the altitude z is increased from 0 to 2000 m on (**a**) the performance curve of the stack and (**b**) the performance map of the compressor.

The gross power of the stack is given as follows:

$$P_{st} = V_{st}(I_{st}) \cdot I_{st} \tag{3}$$

where V_{st} is the stack voltage, which is calculated from the stack current I_{st} by digitalizing the curve of Figure 10a.

The parasitic power of the compressor is calculated by neglecting air humidity and modeling dry air as an ideal gas:

$$P_{comp} = G_{air} c_p T_a(z) \cdot \frac{\left[\left(\frac{p_c}{p_a(z)} \right)^{\frac{k-1}{k}} - 1 \right]}{\eta_c} \tag{4}$$

where $T_a(z)$ and $p_a(z)$ are the temperature and pressure of atmospheric air at altitude (z), respectively. G_{air} is the mass flow rate of air to the cathode, c_p and k are the specific heat at constant pressure and the ratio of specific heats, respectively. η_c is the compressor efficiency, inclusive of isentropic efficiency, mechanical efficiency, and the electric efficiency of the motor. The isentropic efficiency is calculated from the compressor map (Figure 10) as a function of the pressure ratio, corrected mass flow rate, and compressor speed. The last two contributions were assumed to be load-independent.

The air usage G_{air} is a function of the stack current [35]:

$$G_{air} = 3.57 \cdot 10^{-7} \cdot \lambda_{air} \cdot I_{stack} \cdot N_c \quad (5)$$

where N_c is the number of cells in the stack and λ_{air} is the stoichiometric ratio assumed constant and equal to 2 in this investigation.

To enter the compressor map, the corrected mass flow rate is calculated as follows:

$$G_{corr} = G_{air} \frac{p_0}{p(z)} \sqrt{\frac{T_{amb}(z)}{T_0}} \quad (6)$$

Similarly, the water production is given as follows:

$$G_{H_2O} = 9.34 \cdot 10^{-8} \cdot I_{stack} \cdot N_c \quad (7)$$

A secondary contribution to parasitic power is given by the liquid cooling circulation pump that was assumed to require a constant power of P_{pump} equal to 100 W.

At each time of the mission, the model calculates the stack current required to achieve the desired power in each phase of the flight by solving the following equation:

$$V_{st}(I_{st}) \cdot I_{st} - P_{comp}(I_{st}, z) - P_{pump} = P_{fc}(i, z) \quad (8)$$

where $P_{fc}(i, z)$ is decided by the energy management strategy of the hybrid electric power system.

The ambient temperature and pressure at altitude z are computed with the International Standard Atmosphere (ISA) model:

$$T_{amb}(z) = T_0 - 6.5\, z \quad (9)$$

$$p_{amb}(z) = p_0 \left(1 - 6.5 \frac{z}{T_0}\right)^{5.2561} \quad (10)$$

where $T_0 = 288.15$ K, $p_0 = 1.013$ bar, and z is the altitude in meters.

In the fuel cell modules adopted in this investigation, the effect of altitude on the stack performance curve can be neglected since the balance of plant includes a compressor that ensures a constant cathode pressure p_c and the flow rate of Equation (5). This is achieved by controlling the rotational speed of the compressor. However, the increase in altitude determines a higher parasitic power and, therefore, an increase in the stack current to match the desired value of $P_{fc}(i, z)$.

To show how the model captures the effect of altitude, the operating points of the stack and the compressor with a constant request of power (15 kW per module) are shown in Figure 10. The altitude is varied from 0 m to 2000 m.

When the altitude increases, to achieve the same cathode pressure, the pressure ratio must be increased. This explains why the operating point of the compressor moves toward the top of Figure 10b. The parasitic power of the compressor increases because of the increased pressure ratio and decreased efficiency.

Moreover, the corrected mass flow rate also grows because the increase in $\frac{p_0}{p(z)}$ is higher than the decrease in the term $\sqrt{\frac{T_{amb}(z)}{T_0}}$ in Equation (6). For this reason, the operating point of the compressor moves to the left in Figure 10b.

To overcome the increased parasitic power with the same net power, the stack current must increase, causing a reduction in the voltage (Figure 10b) and in the gross efficiency of the stack.

The plot in Figure 11 shows that by increasing the flight altitude from 0 to 2000 m, the parasitic power of the compressor increases from 8.8% at sea level to 12.7% at 2000 m of the gross power. This result is coherent with the reduction in efficiency and net fuel cell power reported in the scientific literature [36].

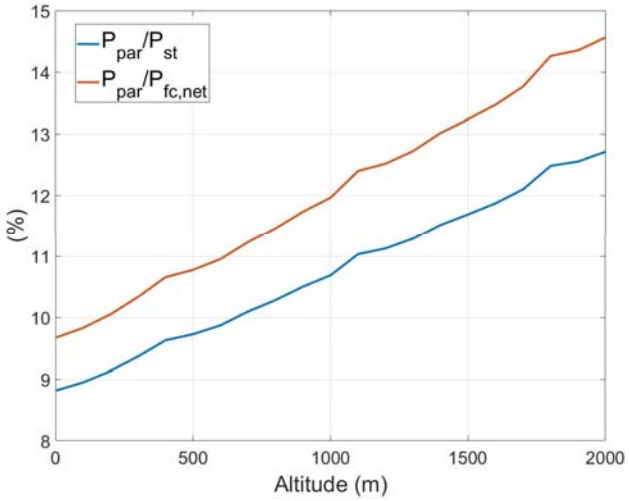

Figure 11. The percentage contribution of the compressor parasitic power to the net and gross power of the fuel cell.

Note that the proposed simplified model does not take into account that the voltage–current curve of the stack is influenced by a certain number of factors, including the stack temperature and the humidity that can be affected by the altitude too. Moreover, the cooling system is assumed to be able to maintain the temperature of the stack at a constant value with the same parasitic power. Finally, the pressure losses in the cathode line are neglected. The level of the analysis, however, is suitable, in the opinion of the authors, for the analysis here described and in relation to similar works in the literature [11].

2.3.2. The Battery Model

Given the battery power requirement at each time step, h, the battery current, I_{batt}, can be calculated by solving the following equation:

$$P_{batt}(h) = [OCV(SOC) - R_i \cdot I_{batt}(h)] \cdot I_{batt}(h) \quad (11)$$

where OCV is the open circuit voltage that depends on the amount of charge in the battery (SOC or State of Charge). The internal resistance R_i depends on the SOC and temperature but can be considered constant in the normal range of variation of these parameters and calculated from the battery datasheet [37]. The state of charge is upgraded at any time during the mission as follows:

$$SOC(h) = SOC_{in} - 100 \cdot \sum_{1}^{N} \frac{I_{batt}(t)}{C} \quad (12)$$

where SOC_{in} is the battery state of charge at the beginning of the mission; C is the nominal capacity of the battery; and N is the total number of time steps (length of the mission). By integrating the battery power, the total electric consumption of the mission E_{tot} was obtained.

3. Environmental Impact Estimate

The environmental impact can be analyzed at different levels. In this investigation, we will define a direct or Tank-to-Wake (TTW) impact on the emissions produced during the operational phase of the aircraft. The emissions associated with the extraction, transportation, and storage of the energy carriers are included in the Well-to-Tank (WTT) impact.

In the original configuration, the combustion of Avgas determines the direct emission of several GHGs (CO_2 and H_2O) and pollutant substances, among which HC, CO, NO_x, and particulate matter are the most relevant. Indirect emissions are also generated in the production from crude oil and in the transportation and delivery of the fuel.

Hydrogen fuel cell systems are generally considered as net zero carbon emission power sources. However, this is only true if the analysis is limited to direct emissions [8]. In fact, one of the main challenges of adopting fuel cells in transportation is the hydrogen production process which can generate a very high Well-To-Wake (WTW) environmental impact. Moreover, in the case of compressed hydrogen vessels, a large consumption of energy is associated with the compression process [10].

From an even broader perspective, a life cycle assessment (LCA) approach should be adopted to consider emissions caused by the manufacturing and disposal of all the components of the power systems. The LCA impact of the fuel cell stack and hydrogen cylinder strongly depends on the catalyst type and load and the materials used for the vessel [18,38]. Therefore, it is difficult to estimate it at the preliminary design stage. Moreover, this study focuses on the energy conversion processes, not on the manufacturing and disposal aspects. Therefore, a complete LCA analysis of the vehicle or the power system is out of scope but will be performed once the detailed project of the power system is complete using available databases like Greet and Gibi, as proposed by Morales et al. [39].

3.1. Direct or Tank-to-Wake Emissions

Direct emissions depend on the emission indexes and the power states of the engine in the six phases of the mission considered in this investigation. The emission indexes measure the amount of a pollutant that is emitted per kg of fuel burned.

3.1.1. Original Configuration

For greenhouse gases, the emission factors for carbon dioxide and water vapor could be found by using mass balance in the complete combustion processes of a hydrocarbon with a value of H/C ratio $a = 2.32$ for Avgas [3]:

$$CH_a + \left(1 + \frac{a}{4}\right) O_2 \longrightarrow \mathrm{CO_2} + \frac{a}{2}\, H_2O \tag{13}$$

where a is the hydrogen-to-carbon ratio of the fuel.

$$EI_{CO_2} = \frac{M_{\mathrm{CO_2}}}{M_{CH_a}} \tag{14}$$

$$EI_{H_2O} = \frac{a}{2}\frac{M_{\mathrm{H_2O}}}{M_{CH_a}} \tag{15}$$

Note that Equation (13) includes the case of hydrogen for $a \to \infty$. M_{CO_2}, M_{H_2O}, and M_{CH_a} are the molar masses of carbon dioxide, water, and hydrocarbon fuel, respectively.

According to [40], a more realistic mass balance should also include CO, SOx, NOx, HC, and soot. While in engines for ground transportation, the mass fraction of such species is quite negligible, in aerospace piston engine combustion is far from ideal, and a large part of fuel carbon is converted into CO and THC (total hydrocarbon) also because of the adoption of a rich fuel mixture. To account for this effect, a carbon fraction can be considered:

$$CO_2 carbon\ fraction = \frac{\mathrm{CO_2}}{total\ C} \tag{16}$$

Yacovitch et al. [3] estimated, for piston engines, a carbon fraction between 0.4 and 0.5, which is much lower than the carbon faction of either turbofan and engines for ground vehicles. The values of the pollutant emission indexes for the Rotax 912ULS proposed by Yacovitch et al. [3], reported in Table 6, are used in this investigation.

Another detrimental effect of using aviation gasoline in the original configuration is the emission of lead. According to [6], 100 Octane Low Lead AVGAS (100LL) emits up to 0.56 g of lead per liter of fuel.

Table 6. Emission intensity (EI) factors [3].

	CO_2	H_2O	HC	CO	NO_x	PM
Unit	kg/kg fuel	kg/kg fuel	g/kg fuel	g/kg fuel	g/kg fuel	g/kg fuel
Takeoff	1.54	1.458	79	808	4.8	0.292
Climb	1.54	1.458	79	808	4.8	0.292
Cruise	1.54	1.458	70.7	795	6.6	0.393
Descent	1.54	1.458	78.9	1062	1.2	0.205
Taxi	1.54	1.458	87.8	819	4.5	0.307
Idle	1.54	1.458	100.9	816	1.6	0.104

3.1.2. Hydrogen Hybrid–Electric Power System

The electrochemical reaction taking place in a fuel cell produces only water as a byproduct. The amount of water produced can be calculated by using Equation (7).

3.2. Indirect Emissions (Production, Compression, and Delivery)

Indirect emissions are associated with the production, compression, and delivery of the energy carriers, namely gasoline for the original configuration, hydrogen in the hybrid electric configuration with the CS operation, and hydrogen and electricity in the case of the CD operation for the new powertrain.

3.2.1. Gasoline vs. Hydrogen

The indirect emission factors of hydrogen estimated by Granovskii et al. [10] were converted into g/kg of fuel and collected in Table 7.

Table 7. Greenhouse gases and pollutant emissions associated with different hydrogen production technologies, inclusive of hydrogen transportation, compression, and delivery compared with gasoline production and delivery [10]. The contribution of hydrogen compression at 200 bar is reported between square brackets.

	Gasoline from Crude Oil	Natural Gas Reforming	Electrolysis from Wind Energy	Electrolysis from Solar Energy
GHGs (kg/kgfuel)	0.53505	10.2	2.47	3.67
[from H_2 compr.]		[0.71]	[1.64]	[1.64]
NOx (g/kg fuel)	0.002784	9.12	2.04	3.00
[from H_2 compr.]		[0.0006]	[0.0001]	[0.0001]
VOCs (g/kg fuel)	0.001044	6.72	0.16	0.24
[from H_2 compr.]		[4.6×10^{-5}]	[0.00136]	[0.00136]
CO (g/kg fuel)	0.000522	3.96	1.68	2.52
[from H_2 compr.]		[0.0005]	[0.0001]	[0.0001]

Note that these values include the operational energy for installation, maintenance, and operation of the power plant in the case of hydrogen produced by electrolysis that is assumed to take place at fueling stations. For hydrogen produced by reforming from natural gas, hydrogen delivery to fueling stations is accounted for, together with natural gas pipeline transportation. For gasoline, the values proposed by Granovskii et al. include crude oil pipeline transportation and distillation and gasoline delivery to fueling stations. Note that the emission factors for VOCs reported by Furuholt [41] for gasoline production with a life cycle assessment method are eight times higher than that calculated by Granovskii et al. but still negligible when compared with the values obtained for hydrogen, especially in the case of natural gas reforming.

In the case of the production of hydrogen from natural gas, a large contribution to emissions is due to pipeline transportation, including compressor stations, independently from the production process.

For hydrogen produced with renewable energy, GHG emissions are mainly due to hydrogen compression. For the other emissions, the contribution of hydrogen compression is negligible, as shown in Table 7.

The values of indirect emissions estimated by Granovskii et al. [10] and reported in Table 7 refer to a storing pressure of 200 bar. From Equation (4), the electric consumption associated with the compression of hydrogen can be assumed to vary with pressure with a factor $\left(\beta_{H_2}^{\frac{k-1}{k}} - 1\right)$, where β_{H_2} is the hydrogen pressure ratio and k is the specific heat ratio of the gas (1.41 for hydrogen). Therefore, the emission factors for GHGs at 350 bar and 700 bar can be obtained by multiplying the values at 200 bar by 1.22 and 1.55, respectively (see Figure 12). The value of 350 bar as hydrogen pressure is the most frequently adopted for similar applications (see Table 1), while 700 bar is the value selected for the proposed hybrid electric configuration [19].

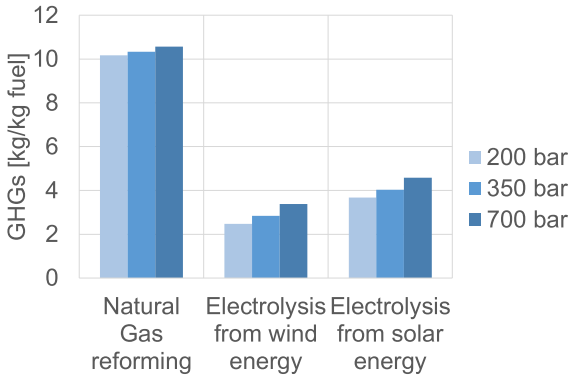

Figure 12. The effect of hydrogen pressure storage on the emission indexes of GHGs.

3.2.2. Electricity

For the indirect environmental impact associated with the charging of the battery in the case of the CS operation, the European electricity mix is considered in this investigation [42].

In Europe, the emissions for the overall production of electricity reached 296 g of CO_2 equivalent per kilowatt hour (g CO_2eq/kWh) in 2019, with 251 g CO_2eq/kWh caused by fuel combustion, 36 g CO_2eq/kWh associated to upstream fuel supply, and 9 g CO_2eq/kWh tied to the construction and decommissioning of electricity plants. [43]. Note that this value decreases in time thanks to the larger exploitation of renewable energy sources. In 2009, a value of 540 g CO_2eq/kWh was reported in the scientific literature [42].

A complete analysis of the indirect emissions of pollutant substances requires a lot of details on the overall electricity production system [44]. The European mix for electricity production in 2022 (see Figure 13) was adopted in this investigation. It was obtained by using the Greet©2023 model developed by the US Department of Energy [45].

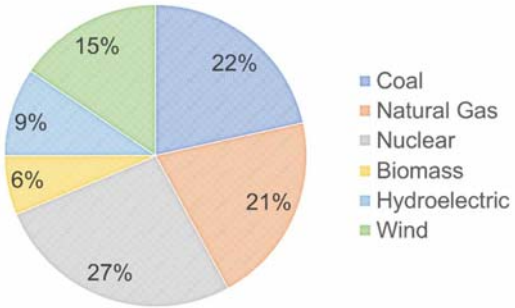

Figure 13. European mix for electricity production.

The emissions indexes for the European mix calculated with Greet©2023 are reported in Table 8. They are inclusive of losses in electric transmission and distribution in Europe [46].

Table 8. Greenhouse gases and pollutant emissions associated with electricity production and distribution (in 2022).

	European Mix
GHG (kg/kWh)	0.337
NOx (g/kWh)	0.3046
VOCs (g/kWh)	0.0393
CO (g/kWh)	0.2136

3.3. Overall Emissions

The WTW, or overall emissions, are obtained by summing the TTW and WTT contributions for equivalent CO_2 and pollutant emissions like NO_x, *CO*, and particulate matter. For the scope of this analysis, the direct emissions of *HC* and the indirect emissions of *VOCs* are summed to obtain the overall *VOCs*, even if the *HCs* from combustion also include non-volatile components.

4. Results

The results of the investigation include a detailed analysis of fuel consumption in the different phases of the flight and the computation of direct and indirect emissions of the two power systems.

4.1. The Consumption of Fuel and Electricity

This section reports the results of the model explained in Section 2 in terms of the consumption of fuel and electricity for the original and new configurations, separately.

4.1.1. Original Configuration

The results of the energy computations for the original configuration with a gasoline engine are summarized in Table 9 in terms of the engine speed and fuel flow rate. The values of the FFR are also reported in Figure 14, together with error bands that represent the minimum and maximum values of the FFR for the same engine in the scientific literature [3,47]. Such error bands are reported as a validation of the proposed simulation approach.

Table 9. Engine and propeller operating points vs. flight phase.

	% of Engine Speed	**FFR (kg/h)**
Takeoff	100%	25.8
Climb 1	82%	18.5
Cruise 1	71%	13.6
Climb 2	89%	21.4
Cruise 2	71%	13.6
Descent	54%	6.7

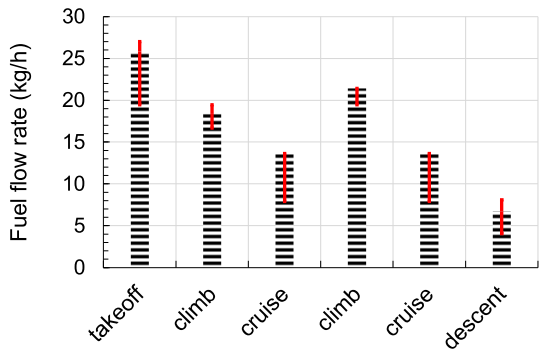

Figure 14. Estimated values of the fuel flow rate, with the error bands (red lines) showing the range of values found in the scientific literature for the same engine [3,47].

The overall consumption of Avgas in the reference flight is 14.4 kg (20 L).

4.1.2. The New Power System

The plots in Figures 15 and 16 show the flight envelope of battery electricity content and hydrogen flow rate as calculated with the proposed model in the case of charge-depleting (left) and charge-sustaining (right) energy management. Thanks to the modular nature of the fuel cell systems, both modules are used only when the required power exceeds an upper threshold power (takeoff and climb). In the other phases of the mission, the fuel cell power is obtained as the sum of the electric power demand and the selected charging power for the battery, which was zero for the CS strategy.

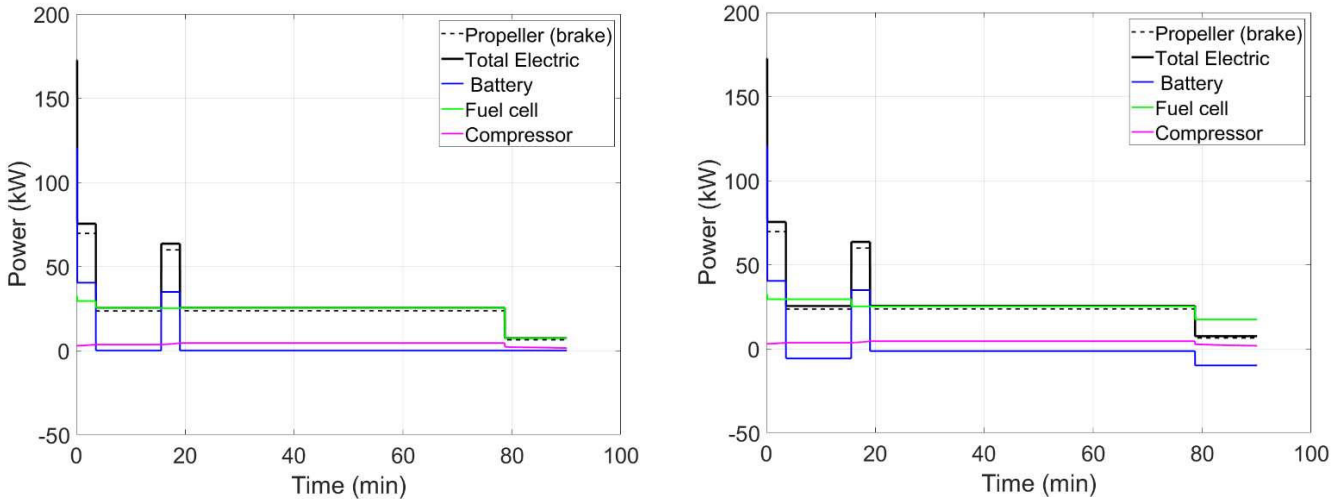

Figure 15. Power requirements during the flight envelop: (**a**) charge depleting and (**b**) charge sustaining.

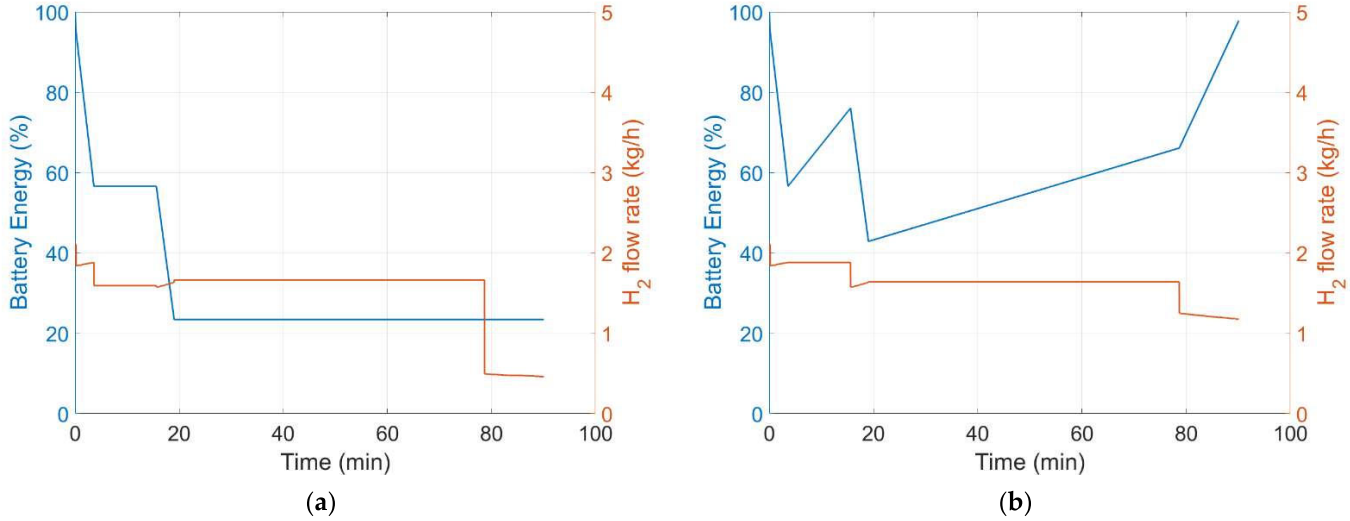

Figure 16. Consumption of hydrogen and battery energy: (**a**) charge depleting and (**b**) charge sustaining.

Figure 15 reports how the power request is satisfied by the two energy sources and shows the auxiliary power as well. The difference between the CD and CS behavior is particularly evident in the last part of the mission (descent), where the fuel cell generates a high surplus of power to charge the battery. However, a minor surplus of power is also generated in the two cruise phases. The effects on the battery energy and hydrogen flow rate of the proposed energy management strategies are shown in Figure 16. Of course, the CS operation is obtained at the expense of a higher consumption of hydrogen. The overall

consumption is 2.25 kg of hydrogen and 4.6 kWh of electricity for the CD case and 2.44 kg of hydrogen for the CS approach.

The CS strategy has the advantages of:

- Avoiding battery charge before the next flight;
- Avoid the operation of the compressor close to the surge line during the descent phase thanks to the higher power requirement of the fuel cell.

The last effect is evident by comparing the working points of the compressor shown in Figure 17.

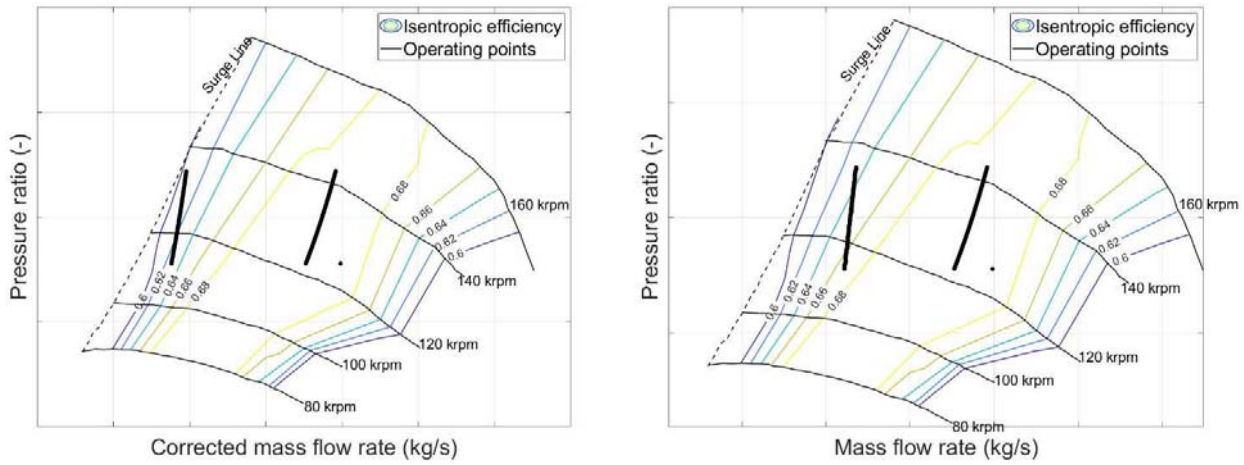

(**a**) (**b**)

Figure 17. Working points of the compressor: (**a**) charge depleting and (**b**) charge sustaining.

Moving the working points away from the pumping line also has the advantage of increasing the compressor efficiency and, therefore, reducing the parasitic power. On the other hand, the use of the fuel cell to charge the battery causes an increase in hydrogen consumption in the CS operation because of two effects: the higher power request and the lower efficiency of the stack, compared with the CD case. The lower efficiency of the fuel cell and the higher efficiency of the compressor are evident in the last 10 min of the flight (descent), as shown in Figure 18, which reports the flight envelop of the motor, fuel cell system, and compressor.

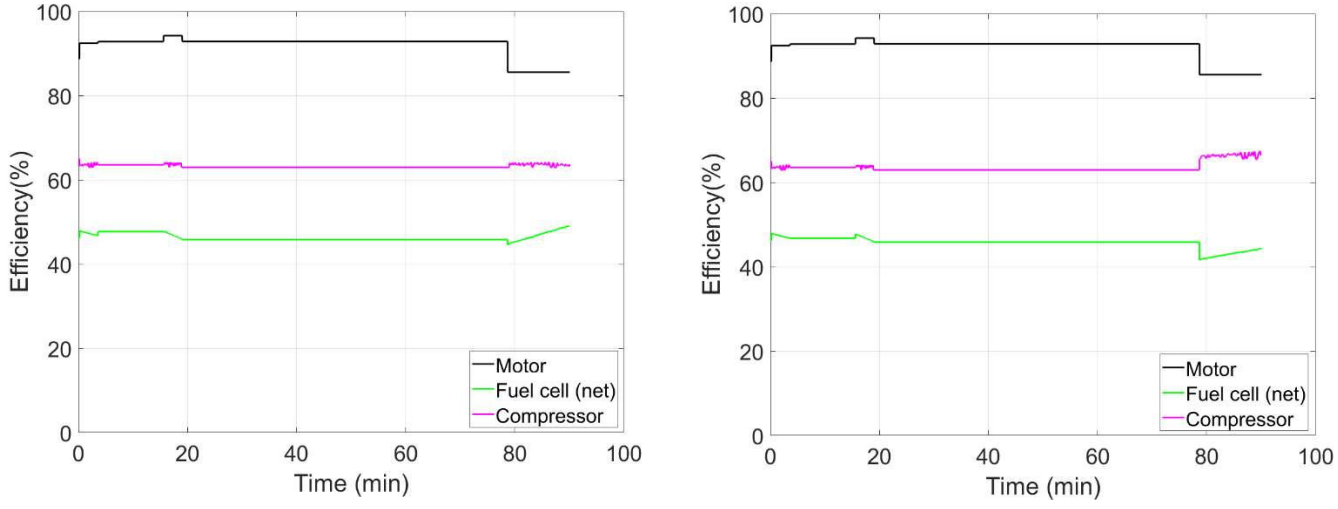

(**a**) (**b**)

Figure 18. The efficiency of the powertrain components: (**a**) charge depleting and (**b**) charge sustaining.

Note that the fuel cell power requirement along the mission is almost constant, especially in the CD operation, thanks to the regularity of the proposed mission. This justifies the adoption of a very simple energy management strategy, while usually more advanced strategies are adopted to avoid abrupt changes in the control inputs of the fuel cell when it operates under dynamic load operations [48].

4.2. Direct Environmental Impact

4.2.1. Original Configuration

The amounts of GHGs (CO_2 and H_2O) and pollutant substances produced in the reference missions with the original configuration are reported in Table 10.

Table 10. TTW emissions of the original configuration.

	CO_2	H_2O	HC	CO	NO_x	PM
	kg	kg	g	kg	g	g
Takeoff	0.48	0.45	0.02	0.28	1.49	0.09
Climb 1	1.17	1.11	0.06	0.69	3.66	0.22
Cruise 1	2.80	2.66	0.13	1.94	12.03	0.72
Climb 2	1.35	1.29	0.07	0.80	4.23	0.26
Cruise 2	14.96	14.19	0.77	10.37	64.25	3.83
Landing	1.41	1.34	0.07	0.79	1.10	0.19
Total	22.16	21.04	1.12	14.86	86.75	5.30

They are the results of the multiplication of the emissions factors reported in Table 6 by the values of the flow rates in Table 9. Of course, the relevance of each phase of the flight to the total emissions is mainly determined by its duration. While in large aircraft, the other phase of the flight can be completely neglected in terms of consumption, the contribution of the non-cruise phases to the overall emissions ranges from 20.5% for *HC* to 12% for NO_x for the ultralight aerial vehicle considered in this investigation. This explains the need to separate the different phases in the calculation of the environmental impact.

Using the emission factor reported in [6], it was estimated that the use of Avgas 100LL in the proposed mission causes the emission of 11.8 g of lead.

4.2.2. The New Power System

The electrochemical reaction taking place in the fuel cell produces only water and heat as by-products. The mass flow rate of H_2O produced by the fuel cell is calculated using Equation (7). The total amount of water produced in the mission is 20.2 kg and 21.7 kg in the case of CD and CS, respectively. Note that a similar value (21.04 kg) is emitted with the original configuration.

4.3. Indirect Environmental Impact

The indirect emissions of pollutant emissions for the two configurations were calculated by considering the emission factors in Table 7 and the consumption of Avgas and hydrogen for the original and new configurations, respectively. For carbon dioxide, the emission factors with a storing pressure of 700 bar (Figure 12) were considered.

The obtained values of these emissions are compared in Tables 11 and 12 for the charge-depleting and charge-sustaining strategies, respectively.

When hydrogen is produced by natural gas reforming, the emissions of all substances are much higher than direct emissions in the original configuration. In particular, the emissions of GHGs are three times larger, while pollutant emissions are three orders of magnitude higher than those for the gasoline configuration.

In the case of hydrogen produced by electrolysis from wind energy, the indirect emissions are lower than those for the original gasoline configuration in terms of equivalent kg of CO_2, but higher in terms of pollutant emissions.

Table 11. Indirect environmental impact: gasoline vs. hydrogen-electric power system with the charge-depleting strategy (inclusive of battery charge).

	Equivalent CO_2 (kg)	*VOC* (g)	*CO* (g)	NO_x (g)
Gasoline (original configuration)	7.72	0.019	0.040	0.008
Natural gas reforming	23.8	15.1	20.5	8.91
Electrolysis from wind energy	7.60	0.35	4.59	3.78
Electrolysis from solar energy	10.3	0.54	6.75	5.67
Battery charge	1.69	0.20	1.07	1.52

Table 12. Indirect environmental impact: gasoline vs. hydrogen-electric power system with the charge-sustaining strategy.

	Equivalent CO_2 (kg)	*VOC* (g)	*CO* (g)	NO_x (g)
Natural gas reforming	24.8	16.4	22.3	9.7
Electrolysis from wind energy	8.2	0.38	4.98	4.1
Electrolysis from solar energy	11.2	0.59	7.32	6.15

For the CS strategy, due to the higher consumption of hydrogen, the indirect emissions are 8% higher than the values in Table 11, but there is no contribution from the battery charge. The indirect emissions in terms of equivalent kg of CO_2 are compared in Figure 19. Note that the contribution of the battery overcomes the benefit of lower hydrogen consumption in the CD case when the hydrogen is obtained from electrolysis using either wind or solar energy. Therefore, the CS strategy appears to be the best in terms of indirect emissions.

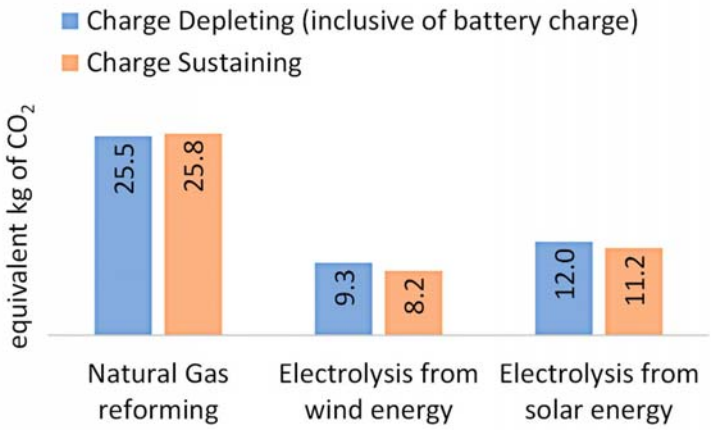

Figure 19. Comparison of indirect impact in terms of equivalent kg of CO_2 for the two energy strategies: CD (inclusive of battery charge) and charge sustaining.

4.4. Overall Emissions

The comparison in terms of overall emissions (WTW) is shown in Figures 20 and 21 in terms of GHGs and pollutant substances, respectively.

The new configuration with the charge-sustaining operation allows a saving of 23.9 kg of CO_2 per flight if hydrogen is produced from electrolysis with wind energy. In the worst case, the charge-depleting operation with hydrogen produced from natural gas reforming, the saving of CO_2 is much lower (5.1 kg per mission).

Note that PEM electrolysis with wind energy was also identified as the best-case hydrogen production scenario based on the results of Lindner [18].

In all cases, the use of hydrogen allows a strong reduction of NO_x and *CO* emissions, while the emissions of *VOCs* in the case of hydrogen produced from natural gas reforming are 12 times higher than the original configuration with gasoline fuel and the piston engine.

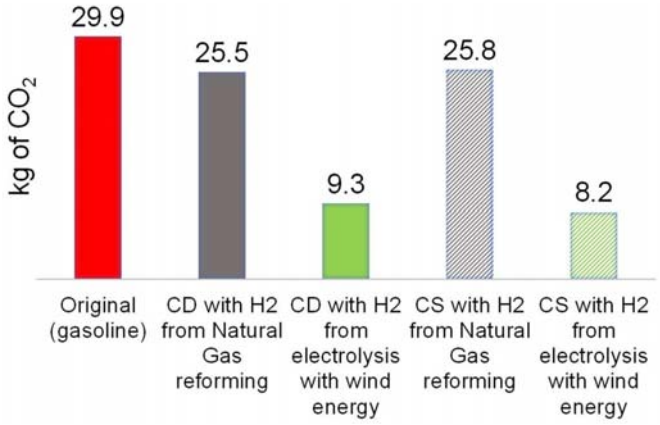

Figure 20. Overall emissions of CO_2: comparison between the original configuration and the proposed hydrogen-based power system.

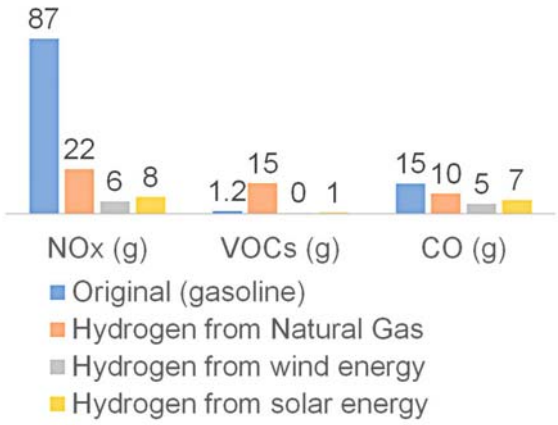

Figure 21. Overall pollutant emissions: original configuration vs. new configuration with the CS strategy.

4.5. Discussion of the Results

Figure 22 puts into evidence the relative performance in terms of greenhouse gases and pollutant emissions of the proposed power systems vs. the original ones by expressing the total emissions in arbitrary units, where 100 au is assigned to the worst configuration for each chemical substance. This plot is useful for addressing the effects of uncertainties and arbitrary assumptions in the present investigation.

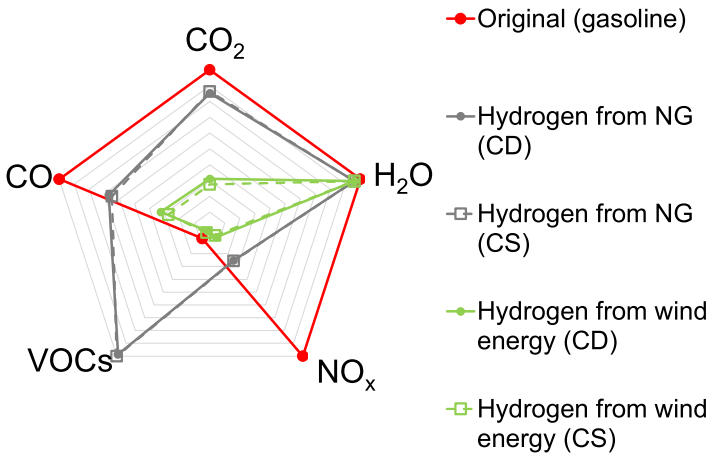

Figure 22. Comparison between emissions in arbitrary units of the original and new power systems.

Note that in terms of *CO* and NO_x, there is a net difference in performance between the original configuration, the new power system with gray hydrogen, and the new power system with green hydrogen produced by electrolysis with wind energy. Therefore, the effect of such uncertainties and arbitrary assumptions (on parameters like the pitch angle, fuel consumption, weight, etc.) should not affect the relative comparison. On the other hand, the emissions of VOCs for the original gasoline configuration and the new power system with green hydrogen are quite close, so hydrogen from wind energy could generate more VOCs under slightly different operating conditions.

The same could be said for CO_2 emissions from the gasoline configuration and the hydrogen produced with reforming from natural gas. In this case, the most critical parameter should be the length of the natural gas pipeline. In the investigation detailed in [10], the same length is considered the same as the crude oil case.

The differences between the CS and CD strategies are affected by the energy mix adopted for electricity production. Since the emission indexes in Europe show a decreasing trend with time, the difference between the two strategies, which is already quite negligible, could easily be canceled out in the near future.

5. Conclusions

In this investigation, a modular fuel cell system hybridized with lithium batteries is proposed and analyzed from an environmental point of view for an ultralight aerial vehicle based on a reference mission of 90 min.

The first step of the investigation was the estimation of the energy flows in the original configuration (Rotax 912UL engine burning Avgas 100LL) and in the proposed power system with a fuel cell. For the second case, two different options were considered for the battery: charge sustaining and charge depleting. With the proposed fuel cell model, the contribution of compressor parasitic power to the gross power of the fuel cell system increases from 8.8% at sea level to 12.7% at 2000 m.

For the original configuration, an overall consumption of 14.4 kg of Avgas was found. However, the mass flow rates were calculated separately for the six phases of the mission for a more accurate evaluation of the environmental impact. For the new power system, the overall consumption of hydrogen was found to be 2.25 kg in the CD operation. The CD strategy requires an additional consumption of 4.6 kWh of electricity to restore the battery energy before the next flight. This is avoided in the CS operation by consuming an additional quantity of hydrogen (0.19 kg) to charge the battery during the lower power phases of the mission. The CS operation has the further advantage of avoiding the operation of the compressor close to the surge line and improving efficiency during the descent phase.

In the second step of the investigation, the direct and indirect emissions produced by the two power systems during the proposed mission are estimated. In terms of direct emissions, the use of hydrogen allows a saving of about 22 kg of carbon dioxide, 1.12 g of *HC*, 15 g of *CO*, 87 g of NO_x, and 5.3 g of particulate matter in the 90 min of the mission. The direct emissions are mainly due to the cruise phase, but the contribution of the other phases is not negligible due to the shortness of the mission, typical of the ultralight application. The same amount of water is produced by the two power systems. The retrofitting of the piston prop aircraft to hydrogen also avoids the emission of lead, which is still used as an additive in aviation gasoline to improve the anti-detonation grade of the fuel.

The data available in the scientific literature for GHG and pollutant emission factors for gasoline, hydrogen produced by natural gas reforming (gray hydrogen), and green hydrogen (electrolysis from renewable energy) were used to estimate the indirect impact of the two power systems. In the case of gray hydrogen, the indirect emissions of GHGs were found to be three times larger, while pollutant emissions are three orders of magnitude higher than the gasoline configuration. The indirect emissions are also higher than the original configuration in the case of green hydrogen produced by electrolysis from wind or solar energy.

Considering the overall Well-to-Wake process, the new powertrain with the charge-sustaining operation saves up to 23.9 kg of CO_2 per flight with the proposed reference mission in the case of hydrogen produced from electrolysis with wind energy. In the worst case, the charge-depleting operation with gray hydrogen, the saving of CO_2 is much lower (5.1 kg per mission). In the proposed case study, a strong reduction of NO_x and CO emissions is obtained with the use of hydrogen with all production paths, but, in the case of gray hydrogen, the emissions of VOCs are much higher than those associated with the use of gasoline in the original configuration with a Well-to-Wake approach.

Author Contributions: Conceptualization, T.D. and L.L.; methodology, T.D.; software, T.D. and A.G.B.; validation, T.D. and L.L.; formal analysis, T.D.; investigation, T.D.; resources, T.D., L.L. and A.F.; data curation, T.D. and A.G.B.; writing—original draft preparation, T.D. and A.G.B.; writing—review and editing, T.D.; visualization, T.D.; supervision, T.D., L.L. and A.F.; project administration, A.F.; funding acquisition, A.F. All authors have read and agreed to the published version of the manuscript.

Funding: This investigation is part of the project "Sviluppo di architetture propulsive ad emissioni zero per l'Aviazione generale (SERENA—CUP: F89J22003510004)," funded by the Italian Ministry for the Environment and Energy Security (MASE), M2-C2-I3.5 call of the Italian Recovery and Resilience Plan. The authors wish to thank the other partners of the project (DTA-Scarl and EngineSoft s.p.a.) for their valuable suggestions and helpful support.

Data Availability Statement: Data not covered by confidentiality agreements will be made available upon request.

Conflicts of Interest: Author Leonardo Lecce is President and CEO of the company Novotech Aerospace Advanced Technology S.R.L. The remaining authors declare that the research was conducted in the absence of any commercial or financial relationships that could be construed as a potential conflict of interest.

References

1. ATI FlyZero. Our Vision for Zero-Carbon Emission Air Travel: Realizing Zero-Carbon Emission Commercial Flight (FZO-ALL-REP-004). 2022. Available online: https://www.ati.org.uk/ (accessed on 2 January 2024).
2. Clean Sky 2. Hydrogen-Powered Aviation: A Fact Based Study of Hydrogen Technology, Economics, and Climate Impact by 2050. 2020. Available online: https://www.euractiv.com/wp-content/uploads/sites/2/2020/06/20200507_Hydrogen-Powered-Aviation-report_FINAL-web-ID-8706035.pdf (accessed on 2 January 2024).
3. Yacovitch, T.I.; Yu, Z.; Herndon, S.C.; Miake-Lye, R.; Liscinsky, D.; Knighton, W.B.; Schoonard, C.; Pringle, P. *Exhaust Emissions from In-Use General Aviation Aircraft (No. Project 02-54)*; The National Academies of Sciences, Engineering, and Medicine: Washington, DC, USA, 2016.
4. Rizvi, S.A.Q.; Kearns, S.; Cao, S. Quantifying the Environmental Impact of Private and Commercial Pilot License Training in Canada. *Air* **2024**, *2*, 162–177. [CrossRef]
5. Available online: https://www.chemeurope.com/en/encyclopedia/Avgas.html (accessed on 2 January 2024).
6. Kumar, T.; Mohsin, R.; Ghafir, M.F.A.; Kumar, I.; Wash, A.M. Concerns over use of leaded aviation gasoline (AVGAS) fuel. *Chem. Eng. Trans.* **2018**, *63*, 181–186.
7. Mills, A.; Peckham, S. Lead exposure from general aviation emissions in the UK: A review and call for action. *Public Health Chall.* **2022**, *1*, e27. [CrossRef]
8. Abdelkareem, M.A.; Elsaid, K.; Wilberforce, T.; Kamil, M.; Sayed, E.T.; Olabi, A. Environmental aspects of fuel cells: A review. *Sci. Total Environ.* **2021**, *752*, 141803. [CrossRef] [PubMed]
9. Baroutaji, A.; Wilberforce, T.; Ramadan, M.; Olabi, A.G. Comprehensive investigation on hydrogen and fuel cell technology in the aviation and aerospace sectors. *Renew. Sustain. Energy Rev.* **2019**, *106*, 31–40. [CrossRef]
10. Granovskii, M.; Dincer, I.; Rosen, M.A. Environmental and economic aspects of hydrogen production and utilization in fuel cell vehicles. *J. Power Sources* **2006**, *157*, 411–421. [CrossRef]
11. Donateo, T. Semi-Empirical Models for Stack and Balance of Plant in Closed-Cathode Fuel Cell Systems for Aviation. *Energies* **2023**, *16*, 7676. [CrossRef]
12. Lapeña-Rey, N.; Mosquera, J.; Bataller, E.; Ortí, F. *The Boeing Fuel Cell Demonstrator Airplane*; SAE Technical Paper, No. 2007-01-3906; SAE: Warrendale, PA, USA, 2007. [CrossRef]
13. Romeo, G.; Cestino, E.; Correa, G.; Borello, F. A fuel cell based propulsion system for general aviation aircraft: The ENFICA-FC experience. *SAE Int. J. Aerosp.* **2011**, *4*, 724–737. [CrossRef]

14. Geliev, A.V.; Varyukhin, A.N.; Zakharchenko, V.S.; Kiselev, I.O.; Zhuravlev, D.I. Conceptual design of an electric propulsion system based on fuel cells for an ultralight manned aircraft. In Proceedings of the 2019 International Conference on Electrotechnical Complexes and Systems (ICOECS), Ufa, Russia, 21–25 October 2019; pp. 1–17. [CrossRef]
15. Rathke, P.; Thalau, O.; Kallo, J.; Schirmer, J.; Stephan, T. Long distance flight testing with the fuel cell powered aircraft Antares DLR-H2. In Proceedings of the Deutscher Luft- und Raumfahrtkongress, Stuttgart, Germany, 10–12 September 2013; p. 301219.
16. Gao, Y.; Jausseme, C.; Huang, Z.; Yang, T. Hydrogen-Powered Aircraft: Hydrogen–electric hybrid propulsion for aviation. *IEEE Electrif. Mag.* **2022**, *10*, 17–26. [CrossRef]
17. Mansouri, H.; Ommi, F. Performance prediction of aircraft gasoline turbocharged engine at high-altitudes. *Appl. Therm. Eng.* **2019**, *156*, 587–596. [CrossRef]
18. Lindner, L. Modelling and Assessment of the Environmental Impacts of a Long-Range Fuel Cell Powered Aircraft. Master's Thesis, University of Rhode Island, Kingston, RI, USA, 2021.
19. Donateo, T.; Ficarella, A.; Lecce, L. Retrofitting of ultralight aircraft with a fuel cell power system. *Eur. Transp. Stud.* **2024**. *in printing*. [CrossRef]
20. Available online: https://avionetaprincipat.com/en/collections/all/rotax-912 (accessed on 19 June 2024).
21. Bauen, A.; Hart, D. Assessment of the environmental benefits of transport and stationary fuel cells. *J. Power Sources* **2000**, *86*, 482–494. [CrossRef]
22. Çalışır, D.; Ekici, S.; Midilli, A.; Karakoc, T.H. Benchmarking environmental impacts of power groups used in a designed UAV: Hybrid hydrogen fuel cell system versus lithium-polymer battery drive system. *Energy* **2023**, *262*, 125543. [CrossRef]
23. Mariscal, G.; Depcik, C.; Chao, H.; Wu, G.; Li, X. Technical and economic feasibility of applying fuel cells as the power source of unmanned aerial vehicles. *Energy Convers. Manag.* **2024**, *301*, 118005. [CrossRef]
24. Donateo, T.; Ficarella, A.; Lecce, L. Preliminary design of a retrofitted ultralight aircraft with a hybrid electric fuel cell power system. *J. Phys. Conf. Ser.* **2024**, *2716*, 012017. [CrossRef]
25. Donateo, T.; Ficarella, A.; Spedicato, L. Development and validation of a software tool for complex aircraft powertrains. *Adv. Eng. Softw.* **2016**, *96*, 1–13. [CrossRef]
26. McCormick, B.W. *Aerodynamics Aeronautics and Flight Mechanics*, 2nd ed.; Wiley: New York, NY, USA, 1995.
27. Donateo, T.; Totaro, R. Hybridization of training aircraft with real-world flight profiles. *Aircr. Eng. Aerosp. Technol.* **2018**, *91*, 353–365. [CrossRef]
28. Available online: https://www.jetexe.com/wp-content/uploads/2015/06/912-ULS-Perfomance.pdf (accessed on 2 January 2024).
29. Donateo, T.; Cavalera, D. Increasing safety in ultralight aviation with a Wankel-based series/parallel hybrid electric power system. *Machines* **2022**, *10*, 486. [CrossRef]
30. Tveitan, S. Life Cycle Assessment of Hydrogen Fuel in Aviation. Master's Thesis, University of Bergen, Bergen, Norway, 2020.
31. Wang, T.; Li, Q.; Wang, X.; Chen, W.; Breaz, E.; Gao, F. A Power Allocation Method for Multi-stack PEMFC System Considering Fuel Cell Performance Consistency. *IEEE Trans. Ind. Appl.* **2020**, *56*, 5340–5351. [CrossRef]
32. Cardozo, J.; Marx, N.; Boulon, L.; Hissel, D. Comparison of multi-stack fuel cell system architectures for residential power generation applications including electrical vehicle charging. In Proceedings of the IEEE Vehicle Power and Propulsion Conference (VPPC), Montreal, QC, Canada, 19–22 October 2015.
33. Marx, N.; Cardozo, J.; Boulon, L.; Gustin, F.; Hissel, D.; Agbossou, K. Comparison of the series and parallel architectures for hybrid multi-stack fuel cell—Battery systems. In Proceedings of the IEEE Vehicle Power and Propulsion Conference (VPPC), Montreal, QC, Canada, 19–22 October 2015.
34. Zhou, S.; Fan, L.; Zhang, G.; Gao, J.; Lu, Y.; Zhao, P.; Wen, C.; Shi, L.; Hu, Z. A review on proton exchange membrane multi-stack fuel cell systems: Architecture, performance, and power management. *Appl. Energy* **2022**, *310*, 118555. [CrossRef]
35. Larminie, J.; Dicks, A.; McDonald, M.S. *Fuel Cell Systems Explained*; Wiley: Chichester, UK, 2003.
36. Haraldsson, K.; Alvfors, P. Effects of ambient conditions on fuel cell vehicle performance. *J. Power Sources* **2005**, *145*, 298–306. [CrossRef]
37. Donateo, T.; Spedicato, L. Fuel economy of hybrid electric flight. *Appl. Energy* **2017**, *206*, 723–738. [CrossRef]
38. Melo, S.P.; Toghyani, S.; Cerdas, F.; Liu, X.; Gao, X.; Lindner, L.; Barke, A.; Thies, C.; Spengler, S.; Herrmann, C. Model-based assessment of the environmental impacts of fuel cell systems designed for eVTOLs. *Int. J. Hydrog. Energy* **2023**, *48*, 3171–3187. [CrossRef]
39. Morales López, J. Fuel Cell-Powered Adaptation of a Light Helicopter Design and Environmental Impact Analysis. Ph.D. Thesis, Universitat Politècnica de València, Valencia, Spain, 2022.
40. Masiol, M.; Harrison, R.M. Aircraft engine exhaust emissions and other air-port-related contributions to ambient air pollution: A review. *Atmos. Environ.* **2014**, *95*, 409–455. [CrossRef]
41. Furuholt, E. Life cycle assessment of gasoline and diesel. *Resour. Conserv. Recycl.* **1995**, *14*, 251–263. [CrossRef]
42. Edwards, R.; Mahieu, V.; Griesemann, J.C.; Larivé, J.F.; Rickeard, D.J. Well-to-wheels analysis of future automotive fuels and powertrains in the European context. *SAE Trans.* **2004**, *113*, 1072–1084.
43. Scarlat, N.; Prussi, M.; Padella, M. Quantification of the carbon intensity of electricity produced and used in Europe. *Appl. Energy* **2022**, *305*, 117901. [CrossRef]
44. Donateo, T.; Licci, F.; D'elia, A.; Colangelo, G.; Laforgia, D.; Ciancarelli, F. Evaluation of emissions of CO_2 and air pollutants from electric vehicles in Italian cities. *Appl. Energy* **2015**, *157*, 675–687. [CrossRef]

45. Wang, M.; Elgowainy, A.; Lee, U.; Baek, K.H.; Balchandani, S.; Benavides, P.T.; Burnham, A.; Cai, H.; Chen, P.; Gan, Y.; et al. *Summary of Expansions and Updates in R&D GREET® 2023 (No. ANL/ESIA-23/10)*; Argonne National Laboratory (ANL): Argonne, IL, USA, 2023.
46. Kelly, J.; Dai, Q.; Wang, M. Globally regional life-cycle analysis of automotive lithium-ion nickel manganese cobalt batteries. *Mitig. Adapt. Strateg. Glob. Chang.* **2020**, *25*, 371–396. [CrossRef]
47. Pisapia, A.M.; Volza, A.; Savioli, T.; Martini, P.; Mattarelli, E. Hybrid-electric power unit for an ultralight aircraft. *J. Phys. Conf. Ser.* **2023**, *2648*, 012081. [CrossRef]
48. Luna, J.; Jemei, S.; Yousfi-Steiner, N.; Husar, A.; Serra, M.; Hissel, D. Nonlinear predictive control for durability enhancement and efficiency improvement in a fuel cell power system. *J. Power Sources* **2016**, *328*, 250–261. [CrossRef]